A Review of Stress Corrosion Cracking/Fatigue Modeling for Light Water Reactor Cooling System Components

S. Mohanty, S. Majumdar, and K.Natesan
Nuclear Engineering Division
Argonne National Laboratory
Argonne, IL 60439

June 2012

A Review of Stress Corrosion Cracking/Fatigue Modeling
for Light Water Reactor Cooling System Components

1. INTRODUCTION

In the United States currently there are approximately 104 operating light water reactors. Of these, 69 are pressurized water reactors (PWRs) and 35 are boiling water reactors (BWRs). In 2007, the 104 light-water reactors (LWRs) in the United States generated approximately 100 GWe, equivalent to 20% of total US electricity production. Most of the US reactors were built before 1970 and the initial design lives of most of the reactors are 40 years. It is expected that by 2030, even those reactors that have received 20-year life extension license from the US Nuclear Regulatory Commission (NRC) will begin to reach the end of their licensed periods of operation. For economic reason it may be beneficial to extend the licenses beyond 60 to perhaps 80 years that would enable existing plants to continue providing safe, clean, and economic electricity without significant green house gas emissions [1]. However, environmental assisted damage and aging issues are some of the major concerns for long-term viability of these nuclear reactors. Despite regular maintenance and tightly regulated operating procedures, aging related failures do occur in US nuclear power plants (NPP).

Different forms of aging might be active in the NPP components [2-7]. They include pure irradiation-induced hardening and softening, irradiation-induced swelling, phase transformation, creep, thermal aging such as thermal hardening and softening of material properties, thermally induced high-cycle and low-cycle fatigue, and high-cycle mechanical fatigue due to flow-induced vibration, chemical corrosion related damage such as flow-assisted general corrosion, crevice corrosion, and stress corrosion cracking (SCC). These mechanisms can act individually or act in combination to accelerate the aging processes. For example, flow accelerated corrosion (FAC), corrosion fatigue (CF), and irradiation-assisted stress corrosion cracking (IASCC) can act in combination with each other to magnify their individual effect. Different NPP components are subjected to different damage mechanisms depending on the type of material used, the way it is manufactured, and the exposure environments. For example, for long-term operation the reactor pressure vessel (RPV) may be subjected to irradiation-induced hardening, swelling, phase transformations, and creep. In addition, reactor pressure vessels may be subjected to fatigue damage. Although fatigue is a degradation mechanism that is second in importance to radiation embrittlement for PWR RPV, it may also affect BWR RPV structural integrity. For example, BWR vessels may be subjected to both high-and low-cycle fatigue [2]. US BWR vessels are designed for low-cycle fatigue based on classical S~N curves, which are based on data generated from in-air fatigue tests. However, research results show that there is an effect of high-temperature (200 to 300°C) oxygenated water (typical BWR environment) on fatigue strength of low alloy steel [8]. This questions the long-term performance of US BWR vessels, which are mostly built using low alloy steel. In addition to the main shells, both the PWR and BWR RPVs contain various nozzles and penetrations. Many of these nozzles are joined to the RPV by dissimilar metal welds that may be affected by stress corrosion cracking and/or corrosion fatigue [2].

Within the pressure vessels, there are many internal structures that support the reactor core,

maintain fuel assembly alignment, etc. These internal structures are not only subjected to reactor coolant water chemistry, but are also exposed to higher temperature and higher irradiation dose compared to the RPV shell. Major possible degradation mechanisms for these internal components are irradiation embrittlement and associated IASCC. In addition, high-cycle fatigue due to flow-induced vibration and low-cycle thermal fatigue are potential causes of aging for long term operation. Thermal embrittlement may also affect some of the internal cast stainless steel components. For example, although most of the PWR internal components are made from stainless steel, some, such as Combustion Engineering design upper guide structure assembly shrouds are made from cast steel grade CF-8. These parts may be subjected to thermal embrittlement and need to be investigated for long term NPP operation.

In addition to the RPV and internal structures, the reactor cooling system (RCS) pipes are part of the reactor coolant pressure boundary whose structural integrity affects the overall functionality of NPP. RCS cooling system pipes include hot leg and cold leg pipes and steam generator tubes for PWR plants and steam, feed water and recirculation pipes for BWR plants, all of which are critical for the overall safety of the reactors. Stress corrosion cracking is a major issue for RCS system pipes particularly in the weld regions where it is connected to RPV nozzles through safe ends. Also, SCC is a major issue for steam generator tube integrity in many US PWRs. The primary cause of SCC is the residual stress created in the component during manufacturing or fabrication processes. For example, high residual stresses are generated during welding of dissimilar metal joints that connect the pipes to RPV shell. Similarly, high residual stresses are generated in steam generator tubes U-bends during its forming process. In addition to SCC, pressure and thermal stress-induced low-cycle fatigue is also a major concern for the RCS. Pressure and thermal stress are created during system transients including heat up and cool down that could cause low-cycle fatigue damage. This fatigue along with SCC leads to corrosion fatigue. For example, SCC/CF can occur in PWR coolant systems nozzles, dissimilar metal welds, and elbows [2]. This review report presents information related to SCC/CF in reactor coolant system piping and weld.

2. RCS COMPONENT MATERIAL, ENVIRONMENT AND STRESS CONDITIONS

SCC/CF in RCS components depends on the material, its associated exposure environment, and the sources of stress. Figure 1 show the parameters that affect the severity of SCC/CF. More details of all these parameters in the context of typical US BWR and PWR NPPs are discussed below.
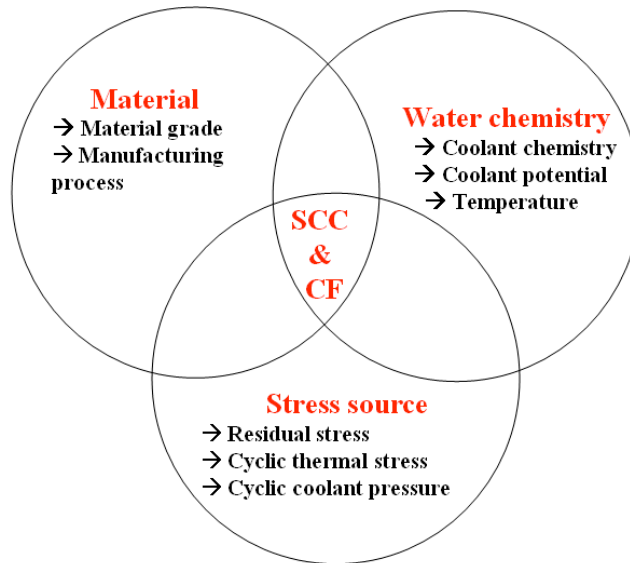
Figure 1. Different parameters affecting SCC/CF

2.1 RCS Component Material and manufacturing process

The reactor cooling system typically includes part of the RPV shell, the RCS piping in or out of the RPV, and the associated nozzles and welds. For PWRs, the major RCS pipes are hot and cold leg pipes and for BWRs the major RCS pipes are steam, feed water, and recirculation pipes.

Reactor Pressure vessel

In general, most of the US NPP reactor pressure vessels are made from low alloy steels. An overview of the types of material and manufacturing processes used in the US NPP RPVs can be found in Shah and Macdonald, 1993 [2]. The older PWR vessels were fabricated from ferritic or low alloy steel plates that were formed and welded to produce the vessel structure. For example, the RPVs of the earliest commercial NPPs, e.g.,Yankee-Rowe (operation in 1961) were made from SA302B steel. Later on, SA533B-1 steel plate became the industry standard. Many of the newer vessels (e.g. Babcock and Wilcox designs) were fabricated from SA508-2 and SA508-3 steel ring forgings rather than plates. The SA508-2 and SA508-3 nozzles of RPV are made by forging. The BWR vessels are also made from low alloy steels. For example, the older BWR vessels fabricated before 1965 used SA302B plates. However, all vessels fabricated since 1965 have used SA533B material. It appears that all the US BWR vessels are made by forming and forging of plates, rather than forged rings. Both the earlier SA302B vessels and the more recent SA508 vessels used A105 II nozzle material (Dresden unit 1). To inhibit general corrosion, interior surfaces of both the PWR and BWR vessels are overlaid with 308 or 309 stainless steel weld material.

Reactor coolant system (RCS) piping and nozzle weld

In the US, the PWR primary system piping is fabricated mostly by three manufacturers -Babcock & Wilcox, Combustion Engineering, and Westinghouse. All these fabricators used different

materials for the RCS piping. For example, the main coolant piping material used by Babcock & Wilcox and Combustion Engineering is wrought ferritic steel. Westinghouse-design used austenitic stainless steel. The combustion engineering piping is constructed of roll-bonded clad plates, whereas Babcock & Wilcox used weld-deposited cladding on the piping inside surface. In the Westinghouse-design, the RCS piping and fitting materials were constructed using both wrought stainless steel and cast stainless steels, such as, Types 304 and 316 wrought stainless steels and CF-8 cast stainless steel grades, respectively. It is to be noted that these grades have similar chemical composition. The piping used in Westinghouse plants is seamless, and because it is fabricated from stainless steel, requires no cladding for corrosion protection. Table 1 shows the details on RCS piping material grades for a typical Westinghouse design PWR.

Table 1. PWR primary RCS piping material [2]

Main piping system			
RPV nozzle forging	Low alloy steel (SA 508-2)		
RPV nozzle safe end forging	Wrought stainless steel (316 SS)		
Piping connected to safe end	Wrought stainless steel (316 SS, 304N SS) & cast stainless steel (CF-8A, CF-8M)		
Safe end to nozzle (dissimilar metal weld)	Weld material	Nozzle butter	Safe end butter
	Stainless steel	Stainless steel	None
	NiCrFe alloy	NiCrFe alloy	None

In the US BWRs, both carbon and low alloy steel material are used for the RCS piping. Table 2 gives the typical piping material information summarized from [2].

Table 2. BWR RCS piping material [2]

Main steam piping system			
RPV nozzle forging	Low alloy steel (SA 508-2)		
RPV nozzle safe end	Low alloy steel (SA 541-1)		
Piping connected to safe end	Carbon steel (SA 155 grade KFC60, cl-1)		
Feed water piping system			
RPV nozzle forging	Low alloy steel (SA 508-2) with stainless steel (308 L SS) clad		
RPV nozzle safe end	Low alloy steel (SA 541-1) with stainless steel (308 L SS) clad		
Piping connected to safe end	Carbon steel (SA 333 grade 6)		
Recirculation piping system			
RPV nozzle forging	LAS (SA 508-2)		
RPV nozzle safe end	Stainless steel (304 or 316 SS) or Nickel alloy (Alloy 600)		
Piping	SS (304 or 316 SS)		
Safe end to nozzle (dissimilar metal weld)	Weld material	Nozzle butter	Safe end butter
	308 SS or 308L SS	309/308/308L SS	None
	Alloy 82/182	Alloy 182	None or Alloy 182

Steam generator tube and support material

In the US PWRs, different types of steam generators are used depending on the plant designer. Westinghouse and Combustion Engineering plants use recirculating steam generators (RSG), whereas Babcock & Wilcox plants use once through steam generators (OTSG). For both RSG and OTSG, the tube material for the older SGs is mill-annealed Alloy 600. The newer SGs use either thermally treated Alloy 600 or Alloy 690 tubes, which are more resistant to SCC than mill-annealed Alloy 600. For Westinghouse and Combustion Engineering designs, the tube support plates and tube sheets are fabricated from either carbon or stainless steel. The Babcock & Wilcox steam generators use tube support plates and tube sheets that are fabricated from carbon or MnMo steel. The tubes are generally meal annealed and is dependent on the manufacturer. For example, Babcock & Wilcox practice was to mill anneal at about 1065 to 1095°C. Following mill anneal, the entire steam generator was subjected to a stress relief heat treatment at about 595°C for about 15 hours. In the case of RSG, the straight tubes are bent to the desired U-bends. Starting from 1970s, Westinghouse followed a thermal stress-relief treatment of tight radius tubes for 15 hours at 705°C to relieve the residual stresses generated in the U-bends due to bend forming.

2.2 Water chemistry

In addition to material properties and manufacturing practice, it is necessary to know the water chemistry of light water reactor for developing predictive damage model. In the predictive model, the water chemistry information can be included as a time dependent field variable. In general, the field variables related to water chemistry parameters are those that are measured for automatic chemical control in the reactor circuit. Tables 3 and 4 show typical PWR and BWR water chemistry, respectively.

Table 3: PWR water chemistry [9]

Water chemistry factors (operational data)	Typical value
pH (at high temperature)	[6.8-7.2]
Conductivity	<30mS/cm
ECP	Not measured
Radiolytic species	
H_2	~2000 ppb
O_2	<5ppb
H_2O_2	<1ppb
Metallic species	
Ni	~1 ppb
Zn (injected)	<50 ppb
Alkali metals	<1 ppb
Li	[0.7-2.2 ppm]
B	[0-2,500 ppm]

Table 4: BWR water chemistry [9]

Water chemistry factors (operational data)	Typical value
pH (at room temperature)	[6-8]
Conductivity	[0.1 to 0.3 μS/cm]
ECP	[-150 to 100 mV]
Radiolytic species	
H_2	~10 ppb
O_2	~200 ppb
H_2O_2	~300 ppb
Metallic species	
Fe	~1 ppb
Cr	~1 ppb
Zn	<1 ppb
Alkali metals	<1 ppb

2.3 Stress source

SCC/CF growth is highly dependent on the presence of mechanical/thermal stress in the component. The stress could be due to residual stress generated during manufacturing process or could be due to applied loading. It is well known that stresses are generated during welding of dissimilar metals. Residual stresses are generated during forming of steam generator tubes. It is necessary to model these manufacturing processes for developing predictive models for SCC/CF. In RCS components, the stress could also be due to thermal loading and coolant pressure. Coolant pressure and temperature cycles during normal operating condition and maintenance/emergency outage transients, the RCS components undergo low cycle mechanical/thermal fatigue. A schematic of pressure and thermal load cycles during normal operating condition and outage are shown in Figure 2. Also, typical PWR and BWR (under normal operating condition) pressure, temperature and flow rate are briefly described below.
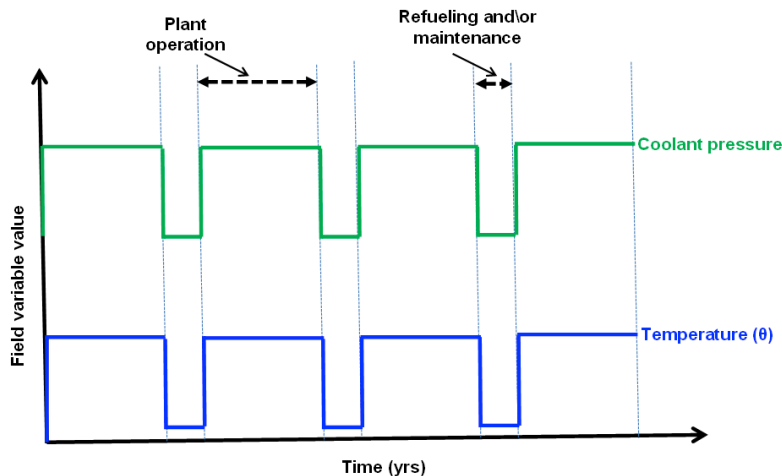

Figure 2. Schematic of pressure and temperature cycle

PWR Pressure, temperature & flow rate

During normal steady state operation, PWR vessels typically experience a pressure of 15.5 MPa and a temperature of 280 to 325°C. The corresponding design pressure and temperature are typically of the order of 17.2 MPa and 280 to 325°C, respectively. The vessel inlet and outlet temperatures vary with the NPP designer. For example, for a 600 MW(e) AP-600 type PWR, the vessel inlet and outlet temperature are 279.5 and 315.6°C, respectively, and the typical primary coolant flow rate is 9940 kg/s. For the secondary loop, the respective nominal condition steam flow rate, steam pressure, steam temperature, feed water flow rate and feed water temperature are 1063 kg/s, 5.47MPa, 272.7°C, 1063 kg/s and 224 °C, respectively.

BWR Pressure, temperature & flow rate

The BWR RPV steady state operating pressure typically varies between 6.90 to 7.24 MPa, whereas the vessel design pressure is 8.62 MPa. The steady state operating temperature typically varies between 282 and 288°C. The core coolant outlet, steam inlet, and feed water temperatures for a typical 1385 MW(e) BWR NPP are 288, 287.8, 278 and 215.6°C, respectively. The corresponding primary coolant flow rate is 14502 kg/s.

3. US PLANT HISTORY RELATED to SCC/CF

The SCC/CF related flaws are a major concern in the US and other world wide NPPs. Many SCC related incidences are reported worldwide. In particular, primary water stress corrosion cracking (PWSCC) is a major concern, because the primary loop is part of the reactor coolant pressure boundary. PWSCC occurs mostly in high residual stress areas, for example, in steam generator tubes and welds in the RPV penetration, nozzles, and other primary piping welds. Some of the historical SCC related incidences reported in US NPPs are briefly described below.

OCONEE, 2001, CRDM nozzle weld cracking [10, 11]

On February 18, 2001, while performing RPV head inspection during a planned maintenance outage at the OCONEE NPP, unit 3, small amount of boric acid residue was found in the vicinity of 9 of the 69 CRDM penetration nozzles. Subsequent nondestructive examinations (NDEs) identified 47 recordable crack indications in these nine degraded CRDM penetration nozzles. The cracks were either axial or below-the-weld circumferential in the CRDM nozzle. The plant administrations concluded that the root cause for the CRDM penetration nozzle cracking was PWSCC. The axial cracking was previously found in PWR CRDM nozzles, however, circumferential cracks above the weld from the OD to the inside diameter (ID) have not been previously identified in the U.S. The potential cause of these new crack findings could be the high residual stresses from initial manufacture and from tube straightening sometimes done after welding. Figure 3 shows a typical CRDM nozzle with weld. The nozzles are constructed from 4-inch OD Alloy 600 Inconel tubes. The nozzles were shrink-fit by cooling to at least minus 140°F, inserted into the closure head penetration, and then allowed to warm to room temperature (70°F minimum). The CRDM nozzles were tack-welded and then permanently welded to the closure head using Alloy 182-weld metal. Shielded manual metal arc welding process was used for both the tack weld and the J-groove weld.
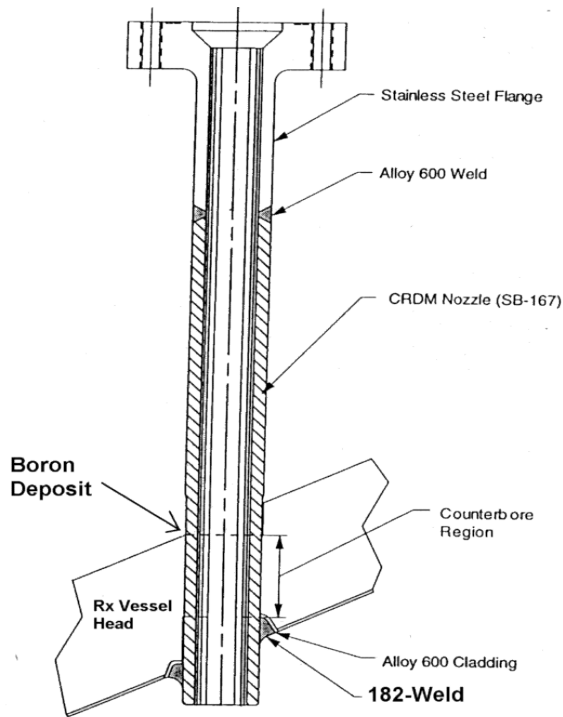
Figure 3. CRDM nozzle penetration

V C Summer, 2000, RPV Nozzle to hot leg pipe weld cracking [12]

On October, 2000, during containment inspection after entering a refueling outage at V.C. Summer NPP, an axial through-wall crack along with a small circumferential crack was found in the first weld between the reactor vessel nozzle and the loop reactor coolant system (RCS) hot leg piping. The crack found was approximately 3 feet from the reactor vessel. PWSCC was suspected to be the main mechanism behind this type of crack formation. High tensile stresses were present in the weld as a result of extensive weld repairs during original construction and these stresses were considered a contributing cause for the PWSCC. The reported pipe material was 304 SS and nozzle material was low alloy steel of SA 508-2 grade. The low alloy steel nozzle was welded using Inconel 182 butter using shielded metal arc (SMA) process. Whereas the main field was fabricated with Inconel weld (82/182) material and using a combination gas tungsten arc (GTA) and the SMA process. Figure 4 shows a schematic of the V.C. Summer nozzle weld.
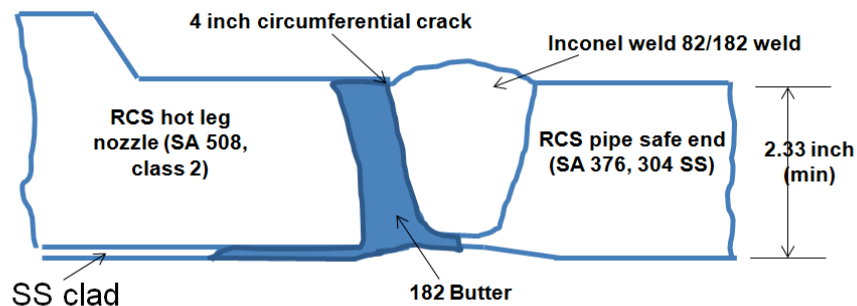

Figure 4. RPV nozzle to hot-leg pipe weld

Other US NPP SCC cases [13]:

There are many other SCC related cracking observed in US NPPs. Some of these cases related to dissimilar metal weld PWSCC are presented here.

In 2006 at *Calvert Cliffs* NPP unit 1, multiple PWSCC related cracks were found in the surge line to hot leg weld and pressurizer relief valve nozzle weld.

During 2006 spring outage at *Davis-Besse*, an axial crack indication of undeterminable depth was found in a cold leg drainline. It is to be noted that, PWSCC has a lower probability to occur at cold leg temperature than at hot leg temperature. Also, in 2006 at *Wolf Creek* NPP during an ultrasound technique inspection drill, five circumferential crack indications were identified in the surge, relief, and safety nozzle-to-safe-end dissimilar metal butt welds. The associated cracking mechanism was attributed as related to PWSCC.

In 2007, at *Farley* NPP unit 2, PWSCC related axial and circumferential cracks were detected in the surge nozzle butt weld. Based on the phased array ultrasound technique inspection, circumferential crack indication of approximately 7.5 cm (3 in.) long (outside diameter dimension), with a maximum depth of 12.7 mm (0.5 in.), which is approximately 33 percent through-wall, was identified at or near the butter-to-dissimilar metal weld interface at or near the inside diameter surface.

In 2008, at the *Davis-Besse* plant, an axial through wall crack was detected in decay heat removal drop line weld. This was detected during a work to install a weld overlay on the drop line. The crack was identified as PWSCC related crack.

In another incident, during a 2008 outage at *Crystal River* unit 3, a circumferential crack was detected in a weld that joins the decay heat removal system drop line to a reactor coolant system hot leg. The detected crack was 38 cm (15 in.) long and the maximum through wall depth was 65% of the wall thickness.

4. SCC/CF PREDICTION USING MECHANISTIC APPROACH

During the past two decades, researchers have tried to develop mechanistic or physics based model to understand and predict stress corrosion cracking (SCC) and corrosion fatigue (CF). However, to date no specific model is completely agreed upon. Many of these models are postulated based on rigorous experimental data. Out of the many SCC/CF models discussed in the literature, the active path dissolution and film rupture model and hydrogen assisted cracking model are the two most popular among SCC/CF research community. The details of these two models are discussed below.

4.1 Active path dissolution and film rupture model

Active path dissolution is a process that involves accelerated corrosion along a narrow path with higher corrosion susceptibility as compared to the overall material or structure. In other words, the overall material is relatively passive and less corrosive compared to the active path. The

active paths generally occur in locations where the corrosion resistant alloying elements are segregated due to manufacturing process. In austenitic steels, the grain boundaries are the possible locations of active paths, because sensitization of the austenitic steel leads to the precipitation and segregation of chromium carbides along the grain boundary. The segregated locations of chromium carbide at grain boundary make these locations less passive and hence more corrosive compared to bulk austenitic steel. Active path dissolution may happen without stress leading to intergranular corrosion that is uniformly distributed over the material. In case of applied or residual stress, the stress helps to open up the cracks, thereby allowing easier transport of corrosion products away from the crack tip and allowing the crack tip to corrode faster. If the accelerated cracking process occurs at the grain boundary, it is called intergranular stress corrosion cracking or IGSCC. Active path dissolution occurs after the protective surface passive oxide layer breaks. This happens due to plastic deformation at crack tip that ruptures the passive film to expose the bare material. The bare metal then corrodes along the active path. One of the earliest SCC model was proposed by Ford and Anderson, 1988, 1989, 1994 [14-16], according to whom, SCC rate relates to dissolution rate at the crack tip where a thermodynamically stable oxide is ruptured by increasing strain in the underlying matrix or base material. The oxide film periodically ruptures and reforms. The periodicity depends on the strain rate in the underlying matrix. The underlying strain is controlled either by creep process under constant load or under cyclic loading. Hence the active path dissolution and film rupture mechanism not only can be used for modeling SCC but also for CF. The crack tip strain rate also can be due to residual stress in the material built up during the manufacturing process. Ford and Anderson [14-16] proposed the active path dissolution and film rupture model based on experimental observations and using Faradic equation of oxidation dissolution under pure chemical corrosion. According to experimental observation, Ford and Anderson proposed the crack growth rate or crack velocity is given as

$$\dot{a} = \frac{da}{dt} = A(\dot{\varepsilon}_{ct})^n \tag{1}$$

where, A and n are two constants related to material and environmental composition at the crack tip. Whereas, the Faradic equation of pure oxidation dissolution is given as

$$\dot{a} = \frac{da}{dt} = \frac{M}{z\rho F} i_t^a \tag{2}$$

where M is the atomic weight, z is the oxidation number, ρ is the density, F is the Faraday constant, and i_t^a is the anodic current density at time t and can be given as

$$i_t^a = i_0^a (\frac{t_0}{t})^n \tag{3}$$

Where i_0^a base metal dissolution rate parameter and t_0 is the repassivation time scaling parameter. From Equations 2 and 3

$$\dot{a} = \frac{da}{dt} = \frac{M}{z\rho F} i_0^a (\frac{t_0}{t})^n = a^*(\frac{t_0}{t})^n \; ; \; a^* = \frac{M}{z\rho F} i_0^a \tag{4}$$

By integrating the above equation over time from $t_0 \rightarrow t_f$ and then averaging the crack growth rate over $t_f - t_0$ the average growth rate can be given as

$$\bar{\dot{a}} = \frac{1}{t_f - t_0} \int \dot{a}\, dt = \frac{a^*}{1-n}(\frac{t_0}{t_f})^n \tag{5}$$

The time per oxide fracture event t_f and can be given as

$$t_f = \frac{\varepsilon_f}{\dot{\varepsilon}_{ct}} \tag{6}$$

where ε_f and $\dot{\varepsilon}_{ct}$ are the oxide film rupture strain and crack tip strain rate, respectively. In the Ford-Anderson model, $\dot{\varepsilon}_{ct}$ is assumed to be constant i.e independent of time. This also means that the time to rupture the oxide film, t_f, is also constant and independent of time. With this assumption, substituting Eq. (6) in Eq. (5) the average crack growth rate can be given as

$$\bar{\dot{a}} = \frac{a^*}{1-n}(\frac{t_0}{\varepsilon_f})^n (\dot{\varepsilon}_{ct})^n \; ; \; a^* = \frac{M}{z\rho F} i_0^a \tag{7}$$

Eq. (7) is the famous Ford-Anderson equation widely used for stress corrosion cracking or corrosion fatigue prediction.

Recently, Hall 2009 A, B [17, 18] has criticized the Ford-Anderson model claiming that the model is derived on the basis of an inconsistent assumption that the crack tip strain rate $\dot{\varepsilon}_{ct}$ is independent of time. According to Hall, the $\dot{\varepsilon}_{ct}$ cannot be assumed independent of time, but rather should be expressed as

$$\dot{\varepsilon}_{ct}(r,t) \; or \; \frac{\partial \varepsilon_{ct}(r,t)}{\partial t} = (\frac{\partial \varepsilon_{ct}}{\partial t})_r + (\frac{\partial \varepsilon_{ct}}{\partial r})_t \frac{dr}{dt} = (\frac{\partial \varepsilon_{ct}}{\partial t})_r + |\varepsilon_{ct}'|\, \dot{a} \tag{8}$$

where $|\varepsilon_{ct}'|$ is the absolute value of negative crack tip strain rate gradient evaluated at the crack tip radius r and $\dot{a} = \frac{dr}{dt}$.

4.2 Hydrogen assisted cracking

This is a process of entrapment of hydrogen atoms into the metal crystal structure and the subsequent local cracking due to local pressure build up. Because of its small size, hydrogen atom dissolves into crystal structure of almost all metals. In addition, the rate of hydrogen embrittlement is accelerated by residual and or applied stress. Hydrogen atoms are usually attracted to a region of high triaxial tensile stress where the metal structure is dilated. Hence they are drawn to the regions ahead of cracks or notches that are under tensile stress. The entrapment of hydrogen atom in the high tensile stress region results in increase in local pressure at the entrapment location. This increase in local pressure results in decrease in energy of cohesion of crystal lattices. This results in further reduction in ductility or further increase in the chance of brittle fracture at the location of hydrogen atom entrapment. In other words, the dissolved hydrogen atoms assist in the fracture of the metal, possibly by making cleavage easier or possibly by assisting in the development of intense local plastic deformation. Hydrogen embrittlement related cracking in metal could be either intergranular or transgranular. In addition, a metal with body-center-cubic (bcc) crystal structure (e.g ferritic steel) is more susceptible to HEC than a metal with face-center-cubic (fcc) crystal structure (e.g austenitic steel). This is because the wider channels between crystallite holes in bcc material atoms than fcc material atoms lead to higher diffusion rate of hydrogen atoms in ferritic steel than in austenitic steel. Because of this, the austenitic steels take a long time to become embrittled by hydrogen atoms compared to ferritic steels. However, hydrogen embrittlement could happen in austenitic steel in combination with active path dissolution at the grain boundary.

Hydrogen embrittlement related stress corrosion cracking have been observed in deaerated, low potential primary water components. In high temperature PWR environment, the cathodic reduction of water provides the crack tip hydrogen pressure necessary for intergranular stress corrosion cracking to occur. At lower temperatures, the coolant-borne hydrogen sustains the crack growth. Hall and Symons, 2001 [19] presented a hydrogen embrittlement SCC model for Ni-Cr-Fe alloy under primary side aqueous environment of a PWR. This model is based on the fact that crack advance occurs by hydrogen assisted creep fracture (HACF) of hydrogen embrittled grain boundaries. According to this model, the crack growth rate can be written as

$$\dot{a} = \frac{r_c}{t} = \frac{r_c}{\left(\varepsilon_f \middle/ \dot{\varepsilon}_{cfz}\right)} = \frac{r_c \dot{\varepsilon}_{cfz}}{\varepsilon_f} \tag{9}$$

where r_c the radius of fracture zone in front of crack tip, $\dot{\varepsilon}_{cfz}$ the strain rate in creep fracture zone and ε_f the critical fracture strain. With the experimental evidence of fracture strain decrease as reciprocal of square root of the grain boundary hydrogen concentration [20] the critical fracture strain ε_f in Eq. (9) can be written as

$$\varepsilon_f = \varepsilon_{f_0}(\frac{C_0}{C_{gb}})^{\frac{1}{2}} \tag{10}$$

where, C_{gb} is the grain boundary hydrogen concentration and ε_{f_0} is the fracture strain at a reference grain boundary hydrogen concentration C_0. Eqs. (9) and (10) can be combined to find

$$\dot{a} = \frac{r_c \dot{\varepsilon}_{cfz}}{\varepsilon_{f_0}}(\frac{C_0}{C_{gb}})^{\frac{1}{2}} \tag{11}$$

5. SCC/CF PREDICTION USING EMPIRICAL MODEL

Currently, there is no single predictive model available that can correctly model SCC and CF. Therefore, empirical models, based on laboratory test data, are currently being used widely for life prediction of LWR components. However, the empirical models are valid only within the range experimental parameters from which they are derived and should be extrapolated with caution. In addition, a model developed based on the testing of coupons made from a particular material may not necessarily be applicable to components made from other materials. To verify the validity of the available empirical models for a particular material environment and to develop new models, multiple large scale testing programs are being conducted in various research laboratories. Some of the SCC/CF related empirical models are discussed below.

One of the earliest SCC crack growth model for LWR components was proposed by Garud and Garber, 1983 [21]. They proposed an empirical model to estimate stress corrosion crack initiation time. According to this model, the cumulative damage a can be estimated using

$$D = \int_0^t A\dot{\varepsilon}^n dt \tag{12}$$

where A and n are m are material constants estimated from a series of constant-extension-rate-tests (CERT) and slow strain rate tensile tests (SSRT). Whereas, the strain rate $\dot{\varepsilon}$ equals to the sum of elastic and nonrealistic strain rates, which are given by

$$\dot{\varepsilon}_e = \frac{\dot{\sigma}}{E} \quad , \quad \dot{\varepsilon}_{ne} = \frac{2D_0}{\sqrt{3}}\exp[-0.5(\frac{Z}{\sigma})^{2n}] \tag{13}$$

where, E is young's modulus, D_0 and n are material parameters, σ is true stress, and Z is the hardness function given by

$$\frac{dZ}{dt} = m(Z_1 - Z)\sigma\dot{\varepsilon}_n \tag{14}$$

where, Z_1 and m are constants. The Eq. 12 used for estimating the time of nucleation and growth to a detectable size. According to this model, crack nucleation occurs when the critical

damage $D_c = 1$. Later Garud, 1990, 1991 [22, 23] proposed a model that can estimate through-wall crack and is give by

$$\dot{a} = \alpha_0 \exp[-\frac{Q}{RT}]\dot{\varepsilon}_{net}^n \ ; \ \dot{\varepsilon}_{net} \leq \dot{\varepsilon}_{cr} \tag{15}$$

Where $\dot{a}$ is the damage growth rate in $\mu m / h$. Based on the Alloy 600 IGSCC test at 365°C reported by Bandy and Rooyen, 1984 [24], Garud estimated following model parameters: $n = 0.5$, $\alpha_0 = 7.338 \times 10^{14}$, $Q = 138.07 \ kJ/mole$, $\dot{\varepsilon}_{cr} = 5 \times 10^{-6}/S$.

Experimental data on SCC growth in Alloy 600 tube specimens were presented by McIlree, 1990 [25]. Based on these test data later Scott, 1991 proposed an empirical model for primary water stress corrosion cracking (PWSCC). The proposed model for Alloy 600 is given as

$$\dot{a} = 1.008 \times 10^{-2}(K_I - 9)^{1.16} \tag{16}$$

where, $\dot{a}$ is the CGR in $\mu m / h$ and K_I is the stress intensity factor in $MP\sqrt{m}$. The above model parameters was estimated based on the experiments performed at 330°C. Later, Foster et al., 1995 [26] proposed a more general model based on arbitrary temperature and is given as below

$$\dot{a} = 9.216 \times 10^9 \exp(-\frac{33000}{RT})(K_I - 9)^{1.16} \tag{17}$$

In the above equation, $R = 1.987 \ cal/mole/K$ is the Boltzmann's constant, and T is temperature in °C. The pre-exponent $9.216 \times 10^9 \exp(-\frac{33000}{RT})$ resembles the form of Faradic equation of anodic dissolution under pure chemical corrosion. The Faradic form can be given as [27],

$$\dot{a} = (\frac{Mi_0}{zF\rho})\exp[\frac{(1-\beta)(E-E_e)F}{RT}] \tag{18}$$

where, M is the atomic weight, z is the number of electrons associated with the anodic process, F is the Faraday's constant, i_0 is the exchange current density, ρ is the density, β is the symmetry factor, E and E_e are the corrosion potential and equilibrium corrosion potential, respectively.

In contrast to Scott's model [28], Rebak and Smilousk, 1995 [29] presented a empirical model that depends not only on stress intensity factor, but also on cold work and pH. The model parameters are estimated using the available experimental data at 330°C for Alloy 600. The estimated model is given as

$$\dot{a} = 4.7 \times 10^{-3} (K_I)^{1.09} (CW)^{0.75} \quad K_I < 30 \; MPa\sqrt{m}$$
$$= 8.4 \times 10^{-3} (K_I)^{0.38} (pH)^{1.67} \quad K_I > 30 \; MPa\sqrt{m} \tag{19}$$

However, the data used to estimate the model parameters considered cold work by bending only and may change for other type of cold work.

Gorman et al., 1994 [30] also presented an empirical PWSCC model to predict life of Alloy 600 components. The model was based on the two-parameter Weibull distribution that estimates the mean time at which 1% of the component population will fail by PWSCC. According to this model the mean time at which 1% of population will fail by PWSCC is

$$t_\% = A t_{ref} \left(\frac{\sigma}{\sigma_{ref}}\right)^n \exp\left[\frac{Q}{R}\left(\frac{1}{T} - \frac{1}{T_{ref}}\right)\right] \tag{20}$$

where A is material constant, n is stress exponent, t_{ref} is time to 1 % failure of a reference case, σ is the total stress at the material surface, σ_{ref} is the reference stress, Q is the activation energy in Kcal/mole, R is the gas constant, T is the absolute temperature, T_{ref} is the reference temperature.

The above-mentioned models are mostly based on tests performed under primary water environment. However, Eason and Nelson, 1994 [31] from EPRI presented an empirical model based on C-ring caustic stress corrosion data. The data generated at Westinghouse and based on both mill-annealed and thermally treated Alloy 600 tube specimens. The model consists of two parts, a probabilistic model of time to crack initiation and a deterministic crack growth rate model. The probabilistic initiation model is based on the two-parameter Weibull distribution and was chosen because of the large scatter in initiation data. The Weibull distribution model for the time to crack initiation is given by

$$F(t_0) = 1 - \exp\left(-\frac{t_0}{\eta}\right)^\beta \tag{21}$$

where, β is the stable parameter and has been found that it is not a strong function of caustic concentration and temperature. However, the parameter η that represents characteristic time strongly depends on temperature T and strain ε. The fitted model for η, with $a_{i=1,2,3}$ as the fitting constants, has the following form:

$$\eta = a_1 + a_2 T + a_3 \ln\left(\varepsilon / 0.002\right) \tag{22}$$

On the other hand, the deterministic crack growth model proposed by Eason and Nelson has the following form:

$$\dot{a} = b_1 + b_1 T + b_3 \varepsilon \quad f \, or \, \varepsilon \geq 0.002$$

$$= \dot{a}|_{\varepsilon = 0.002} \, (\frac{\varepsilon}{0.002}) \, f \, or \, \varepsilon < 0.002 \tag{23}$$

In recent years, research related to SCC and CF has been carried out at Argonne National Laboratory. Majumdar and Natesan, 2011[32] presented a detail review of those works. For example Chopra, et al., 2001 [33] presented a corrosion fatigue crack growth prediction model based on Alloy 600 and Alloy 690 experimental data. The proposed model is based on the in air fatigue CGR model proposed by James and Jones, 1985 [34] and CGR model under LWR environment by Shoji, 1985 [35]. The in air CGR model suggested by James and Jones has the following form

$$\dot{a} = C(T)F(f)S(R)(\Delta K)^n \tag{23}$$

where, $C(T)$, $F(f)$, and $S(R)$ are temperature, cyclic frequency and stress ratio dependent constants, respectively. Whereas, K and n are the stress intensity factor and power law exponent material constant. All the constants in Eq. 23 have to be estimated from experimental data. Based on Eq. 23, Chopra, et al., 2001 [33] in their study on Alloy 600 in air test data found that for the temperature range of room temperature to 538°C the frequency or rise time has little effect on CGR. This assumption leads to $F(f) = 1$ in Eq. 24. However, the value of exponent n is estimated as 4.1 and the temperature and load ratio constant dependent constant C(T) and S(R) are respectively given for Alloy 600 as

$$C_{600}(T) = 4.835 \times 10^{-14} + (1.622 \times 10^{-16})T - (1.490 \times 10^{-18})T^2 + (4.355 \times 10^{-21})T^3 \tag{24}$$

and

$$S_{600}(R) = (1 - 0.82R)^{-2.2} \tag{25}$$

Similarly, for Alloy 690, Chopra, et.al., suggested the equivalent in-air condition $C_{690}(T)$ as

$$C_{690}(T) = 5.423 \times 10^{-14} + (1.83 \times 10^{-16})T - (1.725 \times 10^{-18})T^2 + (5.490 \times 10^{-21})T^3 \tag{26}$$

However, due to limited availability of data, , Chopra, et.al. assumed the frequency constant F(f) and load ratio constant S(R) to be the same as those for Alloy 600. The above equations are valid for in air fatigue condition. For LWR environment, considering high purity water with ≈300 ppb DO, Chopra, et.al. estimated using the following CGR prediction model for alloy 600.

$$\dot{a}_{env} = \dot{a}_{air} + A(\dot{a}_{air})^m \quad with \, A = 4.4 \times 10^{-7}, \, m = 0.33 \, f \, or \, Alloy \, 600 \tag{27}$$

6. SUMMARY AND FUTURE DIRECTIONS

6.1 Summary

The literature review can be summarized as follows:
a) Stress corrosion cracking and corrosion fatigue due to thermo-mechanical cyclic loading could be a major concern for reactor coolant system components.
b) The critical locations for SCC and CF are dissimilar material weld at RPV nozzle and pipe safe end joint, elbow, etc.
c) Active path dissolution combined with film rupture model and hydrogen embrittlement model are the two popular models that suitably explains SCC/CF mechanism.
d) Many empirical models and experiment data are available for reactor component base metals, but few model/data are available for dissimilar metal welds.

6.2 Future directions

Based on this literature survey, ANL has the following future plans:

a) Concentrate on modeling and experimental activities on RCS component base and weld metals.
b) Develop coupon level SCC/CF model for RCS component **base metal** and validate through experiment.
c) Develop coupon level SCC/CF model for RCS component **similar metal weld** and validate through experiment.
d) Develop coupon level SCC/CF model for RCS component **dissimilar metal weld** and validate through experiment.

Reference

1. Nuclear energy research and development roadmap: Report to congress, US DOE, April 2010.
2. V.N. Shah, P.E. MacDonald, Aging and Life Extension of Major Light Water Reactor Components, Elsevier Press, 1993.
3. Light Water Reactor Sustainability Research and Development Program Plan, INL Document, INL/MIS-08-14918, September 2009.
4. J.T. Busby, R.K. Nanstad, R. E. Stoller, Z. Feng, and D.J Naus, " Materials Degradation in Light Water Reactors: Life After 60," ORNL Report, ORNL/TM-2008/170, 2008.
5. G. R. Odette and G. E. Lucas. *Embrittlement of nuclear reactor pressure vessels*. J. of Mater. 53 18–22, 2001.
6. Allen T. R., and J. T. Busby, "Radiation Damage Concerns for Extended Light Water Reactor Service," *Journal of Materials*, Vol. 61, No. 7, July 2009.
7. O.K. Chopra, A.S. Rao, A review of irradiation effects on LWR core internal materials - Neutron embrittlement, 409(3), pp 235–256, 2011.
8. Hans-Peter Seifert, Stefan Ritter, Research and Service Experience with Environmentally-Assisted Cracking in Carbon and Low-Alloy Steels in High-

Temperature Water, SKI Report 2005:60, Laboratory for Materials Behavior, SWITZERLAND, 2005.

9. IAEA-TECDOC-1505, Data processing technologies and diagnostics for water chemistry and corrosion control in nuclear power plants, IAEA, Vienna, 2005.

10. U.S. NRC Information Notice 2001–05, "Through–Wall Circumferential Cracking of Reactor Pressure Vessel Head Control Rod Driver Mechanism Penetration Nozzle at Oconee Nuclear Station, Unit 3," April 30, 2001.

11. U.S. NRC Bulletin 2001–01, "Circumferential Cracking of Reactor Pressure Vessel Head Penetration Nozzles," Aug. 3, 2001.

12. U.S. NRC Crack in Weld Area of Reactor Coolant System Hot Leg Piping at V. C. Summer (Information Notice 2000-017, 2000; Supplement 1, 2000; Supplement 2, 2001). Washington, DC: U.S. Nuclear Regulatory Commission.

13. NRC regulatory issue summary 2008-25 Regulatory approach for primary water stress Corrosion cracking of dissimilar metal butt welds In pressurized water reactor primary Coolant system piping, ML081890403, 2008.

14. F. P. Ford and P. L. Andresen, Development and Use of a Predictive Model of Crack Propagation in 304/316L, A533B/A508, and Inconel 600/182 Alloys in 288°C Water, Proc. 3rd Int. Symp. Environmental Degradation of Materials in Nuclear Power Systems-Water Reactors, Traverse City, MI, The Metallurgical Society/AIME, Warrendale, PA, pp. 789-800, 1988.

15. P. Ford, P. Andresen, H. Solomon, G. Gordon, S. Ranganath, D. Weinstein, and R. Pathania, Application of Water Chemistry Control, On-Line Monitoring and Crack Growth Rate Models for Improved BWR Material Performance, Proc. 4th Int. Symp. on Environmental Degradation of Materials in Nuclear Power Systems-Water Reactors, Jekyll Island, GA, NACE, Houston, TX, pp. 4-26 to 4-51, 1989.

16. P. L. Andresen and F. P. Ford, Fundamental modeling of environmental cracking for improved design and lifetime evaluation in BWRs, Int. J. Press. Ves. & Piping, 59, pp 61-70, 1994.

17. M.M. Hall Jr, Film rupture model for aqueous stress corrosion cracking under constant and variable stress intensity factor, Corrosion Science, 51, 225–233, 2009.

18. M.M. Hall Jr, Critique of the Ford–Andresen film rupture model for aqueous stress corrosion cracking, Corrosion Science, 51, 1103–1106, 2009.

19. M.M. Hall Jr and D. M. Symons, Hydrogen assisted fracture model for low potential stress corrosion cracking of Ni-Cr-Fe Alloys, Chemistry and Electrochemistry of Stress Corrosion Cracking," Ed., R.H. Jones, The Minerals, Metals & Materials Society, Warrendale, PA, pp. 447-466, 2001.

20. D. M. Symons, A comparison of internal hydrogen embrittlement and hydrogen environment embrittlement of X-750, Volume 68, Issue 6, pp. 751–771, 2001.

21. Y. S. Garud and T. L. Gerber, Intergranular Stress Corrosion Cracking of Ni-Cr-Fe Alloy 600 Tubes in PWR Primary Water-Review and Assessment for Model Development, EPRI Report NP-3057, Electric Power Research Institute, Palo Alto, CA, 1983.

22. Y. S. Garud, An Incremental Damage Formulation for Stress Corrosion Cracking and Its Application to Crack Growth Interpretation Based on CERT Data, Corrosion, Vol. 46, pp. 968-974, 1990.

23. Y. S. Garud, An Incremental Damage Formulation and Its Application to Assess IGSCC Growth of Circumferential Cracks in a Tube, Corrosion, Vol. 47, pp. 523-527, 1991.

24. R. Bandy and D. van Rooyen, Stress Corrosion Cracking of Inconel Alloy 600 in High-Temperature Water -An Update, Corrosion, Vol. 40, pp. 425-430, 1984.

25. A. R. McIlree, R. B. Rebak, and S. Smialowska, Relationship of Stress Intensity to Crack Growth Rate of Alloy 600 in Primary Water, Int. Symp. on Contribution of Materials Investigation to the Resolution of problems encountered in PWR Plants. Fontevraud If, Vol. 1, pp. 258-267, 1990.

26. P. M. Scott, An Analysis of Primary Water Stress Corrosion Cracking in PWR Steam Generators, Proc. of the Specialists Meeting on Operating Experience with Steam Generators, Brussels, Belgium, pp. 5-6, 1991.

27. J. P. Foster, W. H. Bamford, and R. S. Pathania, Initial Results of Alloy 600 Crack Growth Rate Testing in PWR Environment, Proc. 7th Int. Symp. on Environmental Degradation of Materials in Nuclear Power Systems-Water Reactors, Breckenridge, CO, NACE, Houston, TX, pp. 25-40, 1995.

28. Gary S. Was, "Fundamentals of Radiation Materials Science: Metals and Alloys

29. Z. Szklarska-Smialowska and R. B. Rebak, Stress Corrosion Cracking of Alloy 600 in High-Temperature Aqueous Solutions: Influencing Factors, Mechanisms and Models, Proc. of Conf. on Control of Corrosion on the Secondary Side of Steam Generators, Airlie Conference Center, Airlie, VA, sponsored jointly by the EPRI and Argonne National Laboratory, NACE, Houston, TX, pp. 223-257, 1995.

30. J. A. Gorman, K. D. Stavropoulos, and A. R. McIlree, Guidelines for Prediction of PWSCC in Steam Generator Tubes, Int. Symp. on Contribution of Materials Investigation to the Resolution of problems encountered in PWRs. Fontevraud III, Vol. 1, pp. 311-318, 1994.

31. E. D. Eason and E. E. Nelson, A Model of Caustic Stress Corrosion Crack Initiation and Growth in Alloy 600, EPRI TR-104073, Palo Alto, CA, 1994.

32. S. Majumdar and K. Natesan, Report on Assessment of Environmentally-Assisted Fatigue for LWR Extended Service Conditions, Argonne National Laboratory, ANL-LWRS-47, 2011.

33. O. K. Chopra, W. K. Soppet, and W. J. Shack, "Effects of Alloy Chemistry, Cold Work, and Water Chemistry on Corrosion Fatigue and Stress Corrosion Cracking of Nickel Alloys and Welds, NUREG/CR–6721, ANL–01/07, 2001.

34. L. A. James and D. P. Jones, *Fatigue Crack Growth Rates for Austenitic Stainless Steel in Air*, in Predictive Capabilities in Environmentally Assisted Cracking, PVP Vol. 99, The American Society of Mechanical Engineers, New York, pp. 363–414, 1985.

35. T. Shoji, Quantitative Prediction of Environmentally Assisted Cracking Based on Crack Tip Strain Rate, Proc. Conf. on Predictive Capabilities in Environmentally–Assisted Cracking, R. Rungta, ed., PVP Vol. 99, American Society of Mechanical Engineers, New York, pp. 127-142, 1985.